Chapter 13
A Neuromorphic, Event-Based, Two-Color Pyrometry for In-process Monitoring of Temperature Change in Welding and Additive Manufacturing

David Mascareñas, Andre Green, Mahtab Heydari, and Allison Davis

Abstract There is currently an increased need to make in-situ measurements of welding and metal additive manufacturing processes to ensure the quality of the resulting fabrications and to predict the resulting mechanical properties. The microstructure of metal parts resulting from these processes plays a large role in determining the resulting mechanical properties. In order to predict the microstructure of these components, it is helpful to measure the solidification rate/time-rate-of-change of temperature in these components. Two-color pyrometry is often used to measure temperature for these types of industrial applications. However, the resulting measurement is often a spatial point measurement or an average over the field of view. It would be preferable to measure temperature changes with high spatial resolution over the entirety of the melt pool and surrounding material in a full-field manner. In prior work researchers have tried to make two- color pyrometry imagers that measure the full-field melt pool, however, these efforts were hampered by the limited dynamic range of conventional 8 bit imagers. Furthermore, the timescales associated with melt pools tend to be on the order of 10^{-3} to 10^{-5} seconds which means that an imager must have a very high frame rate to capture the phenome of interest. Furthermore, the imager would generate large amounts of data that subsequently need to be stored and processed. This large data generation can be impractical on the shop floor. In this work we present a path towards the use of high dynamic range, high-speed, efficient sampling neuromorphic change detection event imagers for the purpose of estimating the time rate of change of melt pool temperatures at high spatial resolution. We anticipate that the development of neuromorphic two-color pyrometer could enable practical in-process monitoring of solidification of melt pools.

Keywords Pyrometer · Dynamic vision sensor · Neuromorphic imager · Event based imager

Introduction

Two-color pyrometry (a.k.a. ratio pyrometry) was originally introduced for the purpose of measuring temperature in a stand-off fashion for the case of unknown emissivity values [1], [2]. Early two-color pyrometers made use of a pair of photodetectors/bandpass filters to capture an average of the "radiative emissions" over the field of view associated with the optics used [3], [4]. These two-color pyrometers were used for measuring the emissions of flames. In 2023 Meyers et al. [5] demonstrated the use of two-color pyrometry with a complimentary metal-oxide semiconductor (CMOS) imager featuring a Bayer filter to sense visible colors. In this work temperature imaging was achieved by examining the ratio of the response for pixels with different Bayer filter color values. The imager was testing in the context of Laser Powder Bed Fusion (LPBF) additive manufacturing. This imager had a number of issues and tradeoffs. First, the pixels were prone to oversaturation, particularly in the middle of the melt pool, making it impossible to recover these temperature measurements. The researchers then tried to reduce saturation by varying the exposure time. However, the researchers report that reducing exposure would reduce the ability to measure the full length of the melt pool. Furthermore, the researchers reported motion blur phenomena in

David Mascareñas · Andre Green · Mahtab Heydari · Allison Davis
Engineering Division, Los Alamos National Laboratory
e-mail: dmascarenas@lanl.gov; andre_green@lanl.gov; mahtabh@lanl.gov; allisonmdavis@lanl.gov

Mahtab Heydari
Department of Mechanical Engineering, Texas A&M
e-mail: mahtabh@lanl.gov

Janko Slavic et al. (eds.), *Computer Vision & Laser Vibrometry, Vol. 6*, Conference Proceedings
of the Society for Experimental Mechanics Series, https://doi.org/10.13052/97887-438-0151-1_13

the measurements when using a longer exposure time. Ultimately the researchers simply ran a single experiment, multiple times over, at different exposure times, in order to try to work around the tradeoffs between pixel saturation, quality of melt pool geometry measurement and motion blur. These mitigation strategies are not suitable for in-process monitoring of melt pool. However, using asynchronous, neuromorphic event-based imagers should greatly mitigate all the current issues with achieving in-process temperature measurements of melt pools.

Background

Asynchronous neuromorphic imagers are fundamentally different than conventional imagers at the hardware level. An event-based imager does not capture individual photographs or frames. Instead, an event based imager only detects information associated with a change in log light intensity value at an individual pixel. Furthermore, this event detection is done directly in hardware at the pixel level. It must be stressed that the event detection is not the result of an image processing algorithm performed on a conventional image. Lichtsteiner [6] provides a representative schematic of the circuit that performs event detection at each pixel that emits events when a change in log light intensity is detected. The data for each event consists of an event timestamp that typically has ∼10s of microseconds accuracy [7] as well as the x-y position of the pixel that detected the event and a polarity value which indicates if the pixel detected an increase or decrease in light intensity. Data is only reported from the imager if the light intensity level at a given pixel changes. Furthermore, only the pixels whose light intensity value has changed report data. If the pixel event data is arranged into the form of a static image, the resulting data looks like a conventional image that has been processed using an edge detection algorithm. Figure 1 shows an example of an office scene consisting of multiple monitors being observed using an event-based imager. The grey background indicates pixels where no data is reported. In contrast, the white and black pixels indicate areas where the light intensity value has either increased or decreased beyond the threshold. Generally the black and white pixel events occur at the edges of objects because this is where the strongest light intensity changes tend to occur. The result of this detection-at-the-pixel approach, is that event-based sensors consume less power, less memory/bandwidth, and they operate across a wide range of timescales and dynamic ranges [6].

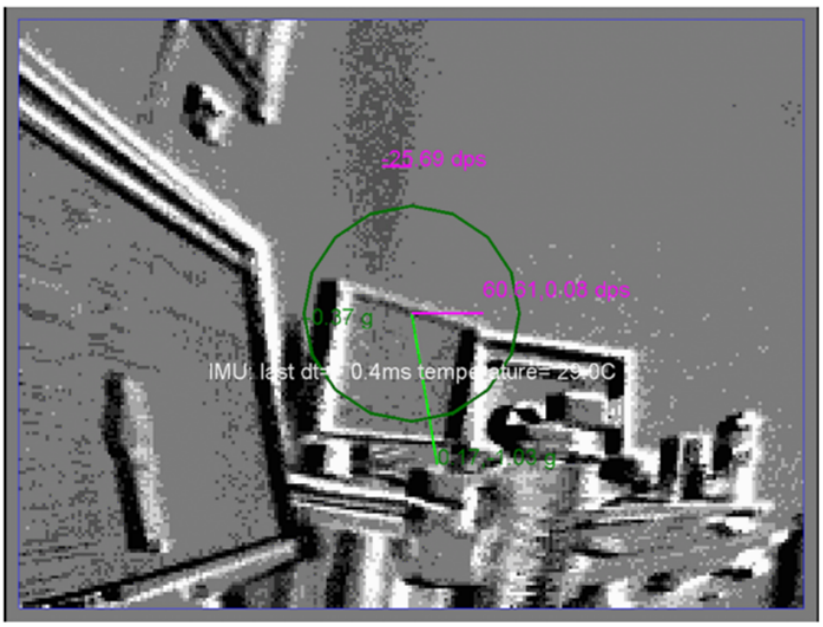

Fig. 1 Example of event data captured from an office scene and formed into a frame [10].

Event imagers have four properties that make them particularly attractive for melt-pool two-color pyrometry. First, the event-detection pixel circuit detects changes in log light intensity which means that imager naturally has a high dynamic range of ∼120 dB, [6], [7]. In prior work the team has found that this high dynamic range is sufficient for observing melt pools [8]. Second event imagers are able to capture phenomena on the sub-millisecond timescale. Conventional high dynamic

range weld cameras [9] have framerates on the order of tens of Hertz which is not sufficient for observing melt pools with sub-millisecond dynamics. Third event imagers are very efficient at sampling. In the case of analyzing data from tests associated with observing laser welding melt pools, these imagers have been observed to require approximately 35 times less memory to store data comparable to that of a conventional imager . These memory savings are important because they can potentially help lead to online process control of AM as well as for making it possible to store more data associated with the process parameters during a build. Currently building components requires storing data files on the terabyte scale of memory which is not amenable to storing, processing or communicating over a network. Fourth, event imagers provide a timestamp for each event recorded with 65 - 200 μs temporal accuracy [7]. The high resolution timestamps opens up interesting possibilities for changing the effective exposure time associated with forming frames from the events to better estimate melt pool geometry and for motion blur control. The concept of the digital coded exposure was introduced by Gothard [8], which allows for arbitrary modification of exposure time using event data in post-processing.

Analysis

Experimental Setup

The prototype neuromorphic two-color pyrometer was is shown in Figure 2. Two DVXplorer silicon retina imagers were attached to a beam-splitter sharing a 100 mm lens (Thorlabs MVL100M23) and aimed at a halogen lightbulb. Note that the 100 mm lens/event imagers are being used in a non-standard configuration such that the image comes into focus when the object is located $\sim$21 centimeters from the front of the 100 mm lens. The field-of-view of this optical setup is slightly less than 10 mm on a side. A green 532 nm band-pass filter (ThorLabs FLH532-10) was placed in the optical path of one imager and a red 650 nm band-pass filter (ThorLabs FBH650-10) was placed in the optical path of the other imager; both filters had a full-width-half-maximum (FWHM) of 10 nm. The filament of a halogen lightbulb served as an approximate blackbody radiator and was exposed to voltages across its terminals at integer voltages in the 5V to 10V range (inclusive).

Figure 3 shows a plot of the response ratio vs temperature for the optical setup associated with our neuromorphic two-color pyrometer. Although the mapping between temperature and the response ratio between the spectrum intensity at 532 nm and 650 nm is non-linear, it is one-to-one and so can be inverted to recover the temperature from the spectrum intensity ratio.

The spectrum emitted by the halogen bulb was approximately black-body, but did not conform perfectly to the theoretical predictions (Figure 4); this may be an effect of our spectrometer's diffraction grating or non-idealities associated with the halogen bulb. Consequently the decision was made to track the peak-intensity wavelength rather than use the temperature of the most-fit the blackbody curve to track changes in the filament temperature.

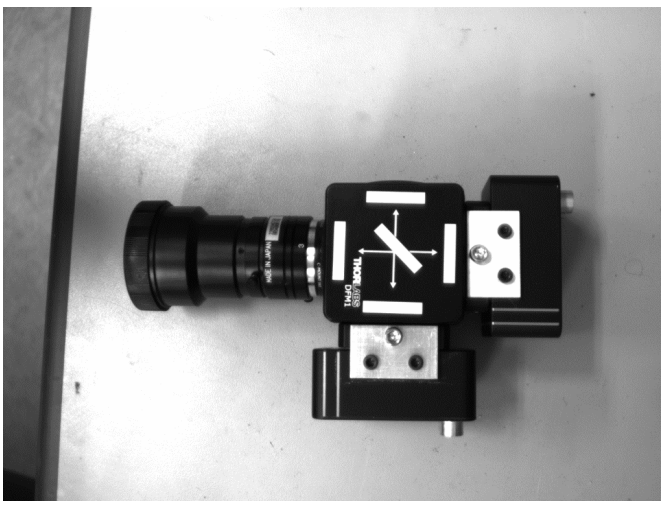

Fig. 2 The beam-splitter (center) has two DVXplorer silicon retina imagers attached (right and bottom); the imager on the right is equipped with a 532 nm filter; the imager at the bottom is equipped with a 650 nm filter. Both imagers see through the beam-splitter to share a 100 mm lens.

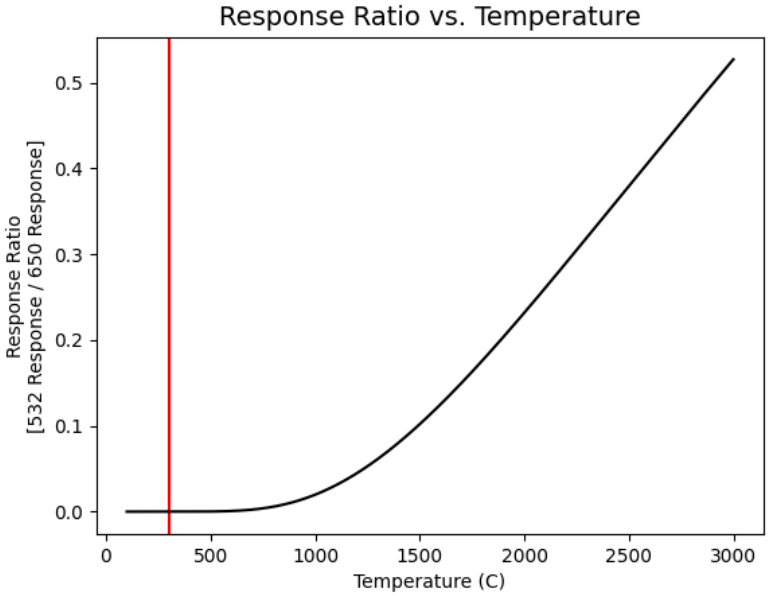

Fig. 3 The mapping between temperature and the ratio of irradiance at 650 nm and 532 nm is invertible.

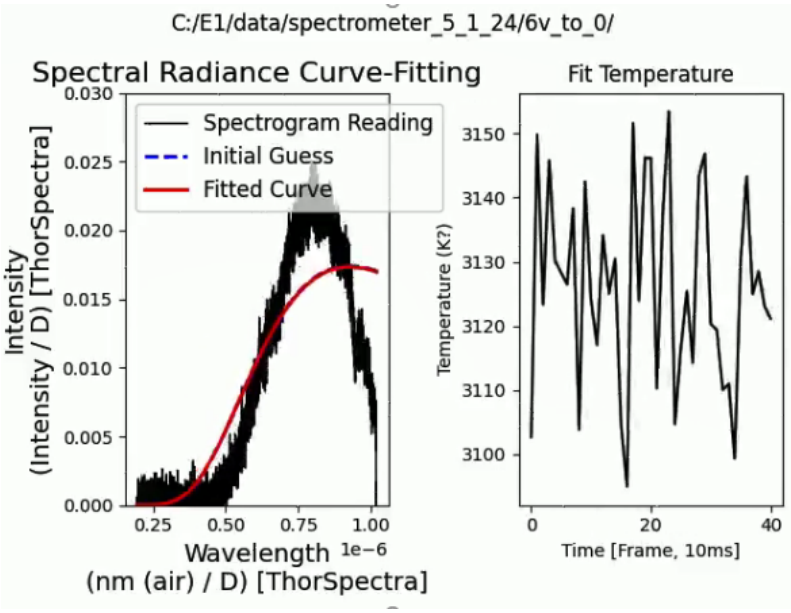

Fig. 4 The mapping between temperature and the ratio of irradiance at 650 nm and 532 nm is invertible.

Experimental Results

Next the wavelength of highest intensity detected by the two-color pyrometer changed in response to the tungsten filament being excited with different voltages is considered. Note, the voltage scale for Figure 5 through Figure 7 is shown in Figure 6. Figure 5 shows the response of the spectrometer to the different initial voltage levels. In these tests the tungsten filament was excited using the specified voltage levels and brought to steady state. Then the voltage was abruptly set to zero in order to induce a temperature change, and thus a light intensity change at the pixels that could be detected using the event-based imagers. Figure 6 shows the event ratio time series associated with the different voltage levels. These ratios are calculated by taking all of the events that occur in the pixels that are associated with the image of the halogen blub. For this initial proof-of-concept the ratio of events at a pixel was used to try to indicate a change in temperature at a pixel or over a set of pixels. Ideally, temperature estimates for each pixel based on the events at that pixel/spatial location should be obtained. However,

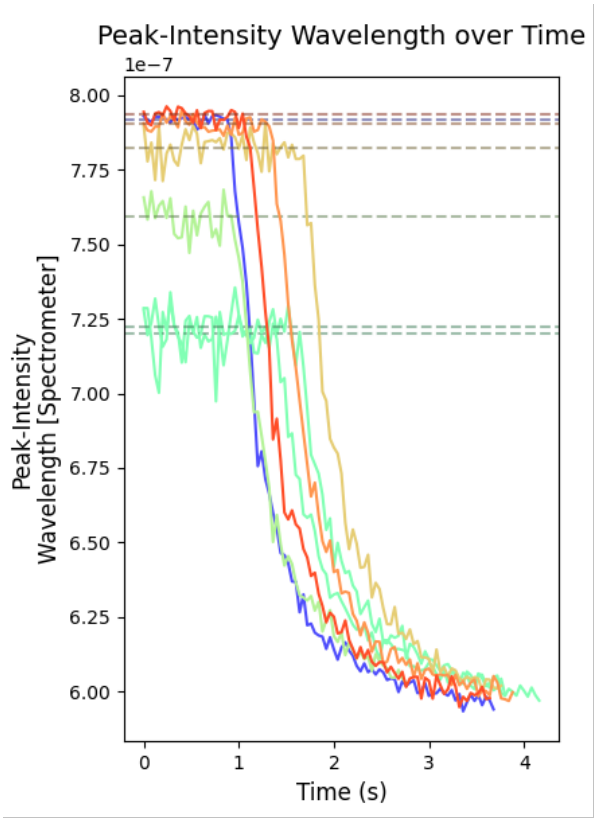

Fig. 5 The spectrogram records different peak intensities for each voltage, with higher peaks for higher voltages as expected. However, the filament appears to reach its peak temperature at 8V.

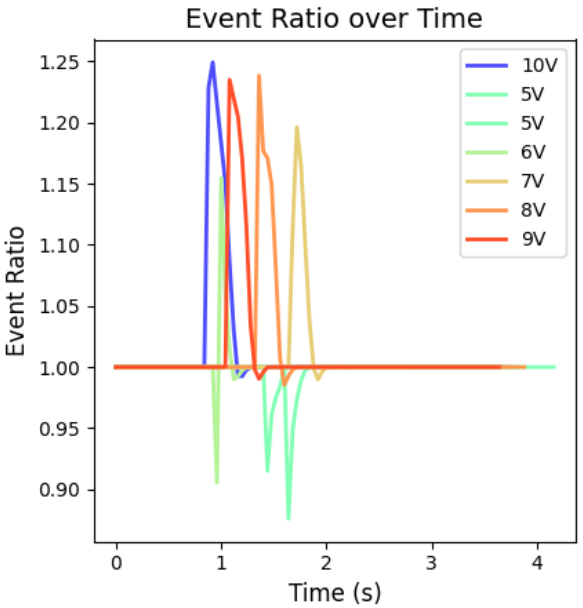

Fig. 6 The event-ratio time-series from each test are overlaid in time. The offsets between the peaks are merely from experimental variation and not of particular relevance.

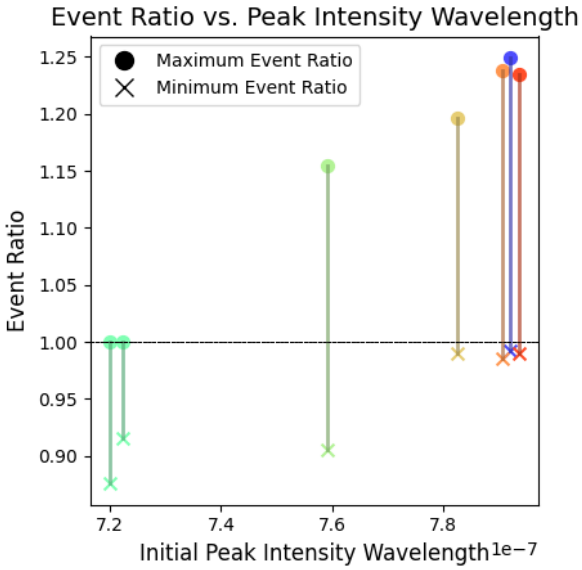

Fig. 7 The minimum and maximum event ratios from each experiment's time-series. The maximum peak intensities for tests above 8V appear saturated as is also seen with the spectrometer.

in initial tests, wide variance in event ratios observed at pixels/spatial locations that should presumably exhibit similar temperature changes, were observed. This observation may be caused by variation in the contrast threshold as mentioned in prior studies of the uniformity of response of pixels in event imagers [6]. To enable per-pixel temperature change estimates it will most likely be necessary to calibrate the imager in order to remove this variance in pixel behavior. The variation in pixel behavior has some similarity to fixed pattern noise in conventional imagers [6].

The wavelength with the greatest intensity as detected by the spectrometer, increases with voltage, although above 9V the response appears to saturate; this may be a limitation of the bulb used. Similarly, the ratio of events between the camera with the 650 nm filter and the 532 nm filter increases as the halogen bulb is supplied a higher voltage (and hence is at a hotter temperature), meaning that the halogen bulb at different temperatures can be differentiated by this method.

At the lowest voltage (5V), events only triggered on a single camera; it is believed that this is because the brightness at 5V was sufficient to trigger events from the 532 nm filtered camera, but insufficient to trigger events from the 650 nm filtered camera. It is also possible this was due to manufacturing variations in the event cameras.

Simulation

In addition to the experimental investigation, a 3D heat-diffusion model was made to test the silicon retina response in simulation. Each pixel of the simulation has an associated temperature; each temperature is mapped to black-body curve; the dot-product of this curve with the frequency-response curve for each simulated 532 nm and 650 nm is the corresponding intensity for the simulated input to the virtual silicon retinas. Then a simulation of the silicon retina response to this irradiance excitation in order to generate events using an approach primarily based on threshold crossings is performed; finally, the ratio of these events is used to estimate the changes in temperature which are combined to generate the final temperature field reconstruction.

In this work the case where the threshold for triggering an event was set at both a low (Figure 10) and high (Figure 11) value is considered.

In simulation, the temperature reconstructions approximate the temperature within the area of interest (within the heated region) well. In both simulated reconstructions, the room-temperature outside border of the region outside the heated area that receives heat is not accurately reconstructed because there is insufficient light being generated by the blackbody radiator to generate events (Figure 12); in future work, this may be rectified with the use of a short-wave infrared (SWIR) event-driven imager.

In the event reconstruction which uses a low event threshold, there is also an issue on the corners within the sample: here the temperature is changing too rapidly for the simulated imager to generate events proportional to the change. A higher threshold can be used to eliminate this issue at the cost of reduced temperature accuracy for slower changes in the center

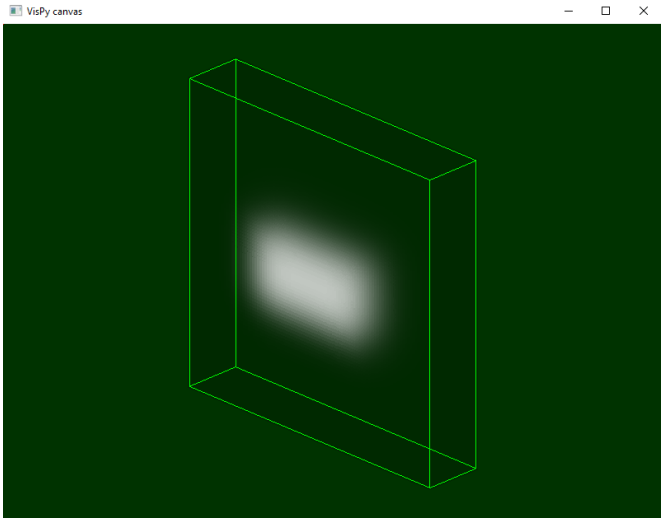

Fig. 8 The 3D heat-diffusion simulation; a block of steel with no cross-medium (air) interaction was used.

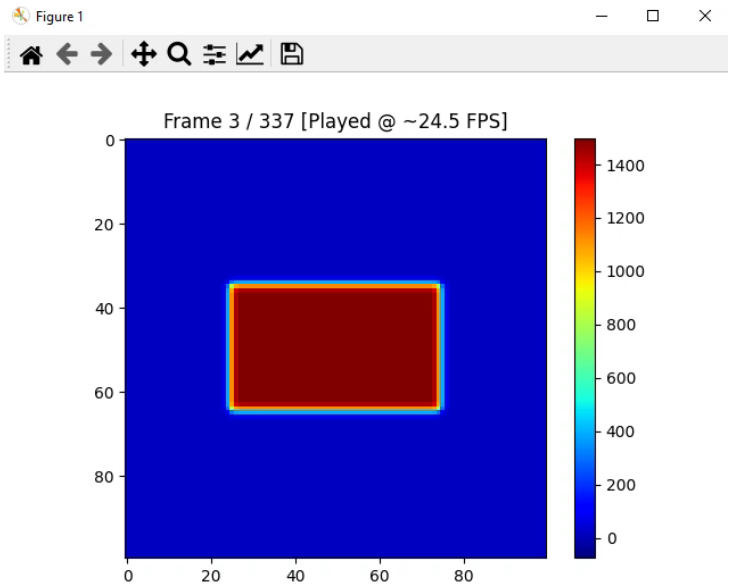

Fig. 9 A 2D view of the top of the simulated sample; this is what would be visible to a thermal imager.

of the heated sample: in short, with a higher threshold the real temperature is changing, but not quickly enough to generate an event such that the reconstruction aligns with the simulation at all times. However, please note, event imagers have a temporal resolution on the order of 65-200 μs [7]. Some of the issues mentioned here, with respect to the simulated imager not being fast enough to generate events, are most likely an artifact of the approach used to generate this simulation and are not necessarily present in observing actual physical systems. Prior work has been done on generating simulations of events, but these techniques typically rely on working from a uniform-in-time simulation framework which is not necessarily well-suited to event-based sensing, and can struggle with phenomena such as noise and the behavior of the arbiter [11], [12], [13]. The problem of simulating event-based imagers is still an open research problem worth of further investigation.

Future Experimental Setup

Simulating the process of event generation is challenging. To alleviate this challenge the researchers developed an alternative sensor-in-the-loop approach wherein the DVXplorer event-imager is coupled with a high-speed monitor (Alienware

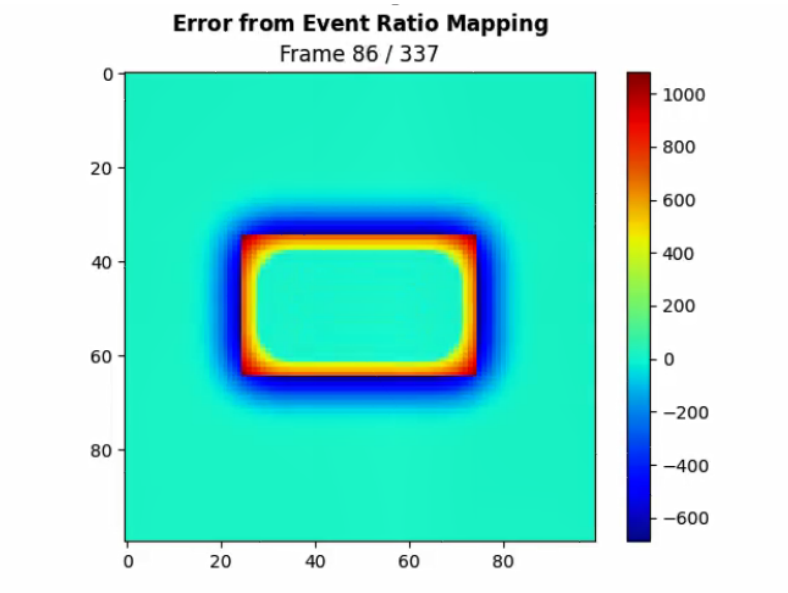

Fig. 10 The error of the reconstruction (using a low threshold for event generation) against the simulated temperature. The inner borders of the heated region cool quickly, over-saturating a low-threshold imager and lead to an over-estimation of temperature.

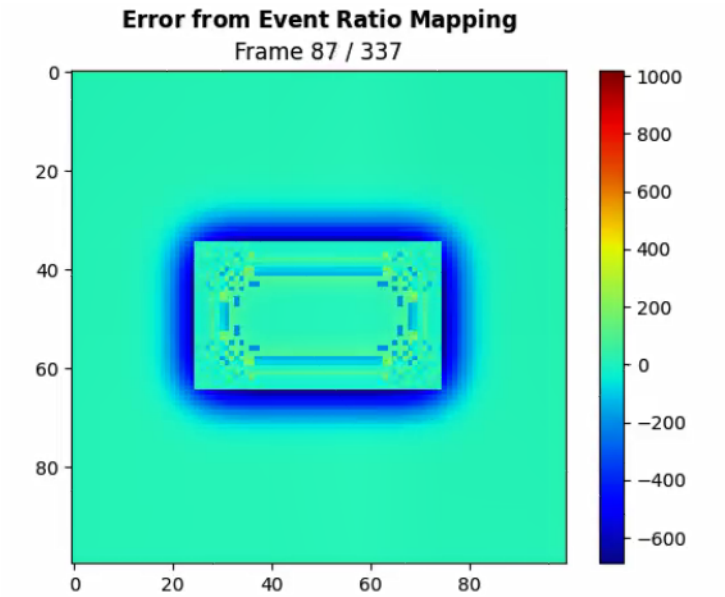

Fig. 11 The error of the reconstruction (using a high threshold for event generation) against the simulated temperature. The issue with the inner borders has been resolved, at the cost of minor error within the regions of the sample whose temperatures change more slowly.

AW2523F, 360 Hz refresh rate) in an optically isolated environment (Figure 13), where a simulation of the desired dynamic experiment (e.g. heat-diffusion) is displayed on-screen. The event-based imager was attached to a beam splitter and mounted to a frame with the front of the beam splitter placed at a distance of 33.5 inches away from the face of the monitor. A 12mm lens was used to observe the monitor using the event imager. The frame used to hold the monitor and imager is of dimensions 23 5/8” x 15 3/4” x 39 1/8”, and the bar holding the imager was set to a height of 5 9/16” above the bottom of the frame. Figure 14 shows examples of a diffusion simulation along with examples of events formed into frames captured by observing high-speed monitor displaying the simulation.

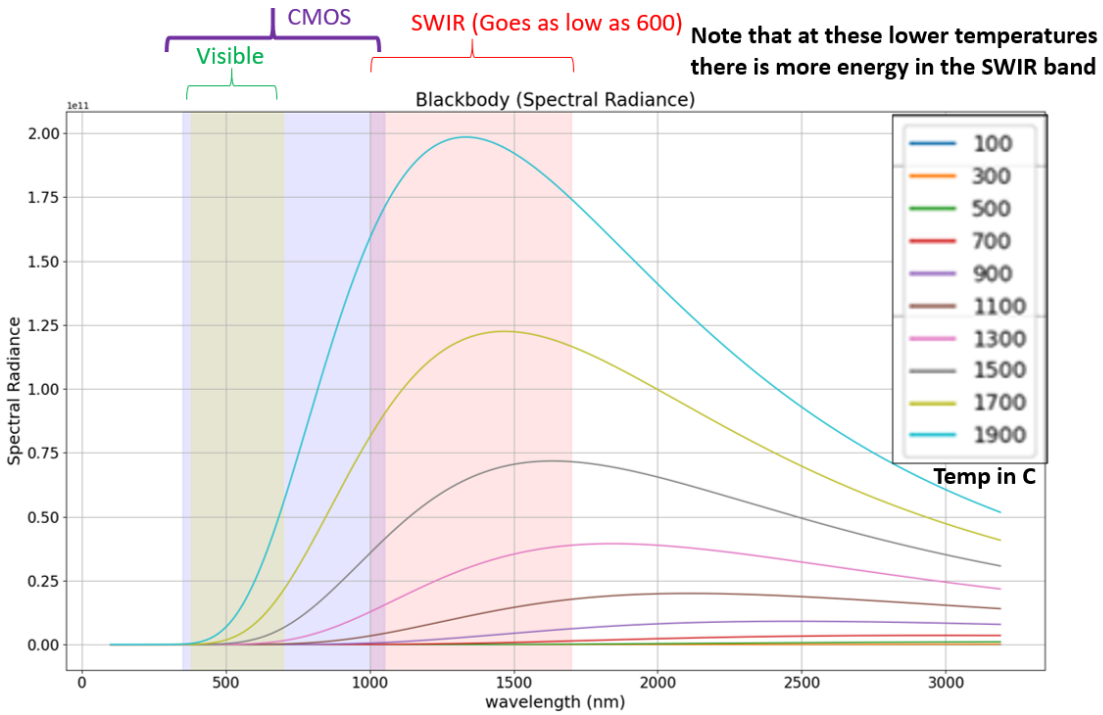

Fig. 12 At low C, the intensity of light at 532 nm and 650 nm is low enough to not be registered by our event-driven imagers; future development of event-based SWIR imagers may rectify this issue.

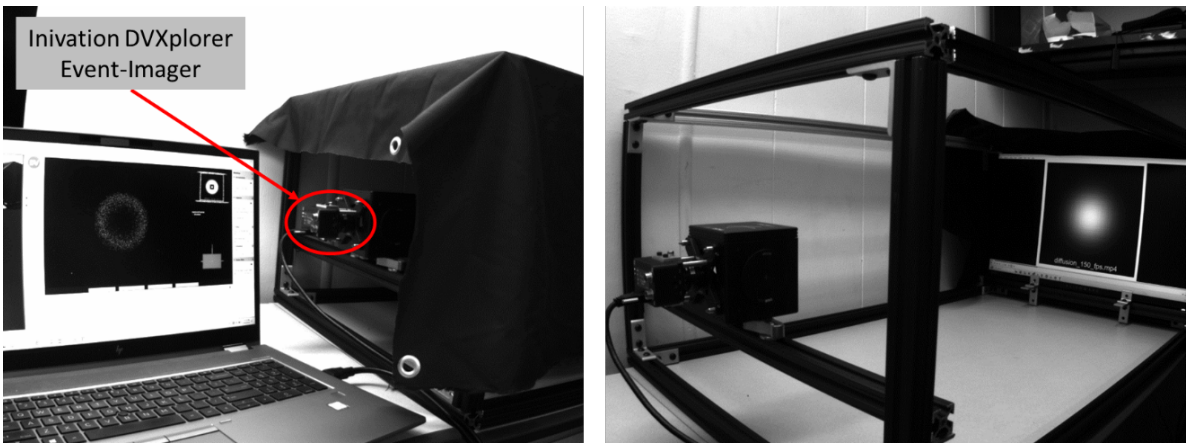

Fig. 13 The future experimental setup; a DVS imager (to be replaced by the beam-splitter assembly shown previously) is mounted on a cage and aimed at a high-speed monitor. The assembly is covered to isolate outside light.

This hybrid sensor-in-the-loop approach can be employed to develop more sophisticated event/image processing algorithms that can better estimate the change in temperature. In addition, this approach should help facilitate providing controlled stimulus to the event imager that can be used to help account for variations in the response of individual pixels. The advantage of this hybrid setup is that the user has full control over the simulation and has access to the full-field ground truth information that led to the events generated by the event imager. The disadvantage of this hybrid setup is that the dynamics that can be emulated is limited by the framerate of the monitor and the dynamic range of the light that can be generated is limited by the light output of the monitor. As such in its current form the hybrid sensor-in-the-loop simulator cannot emulate high light intensity environments.

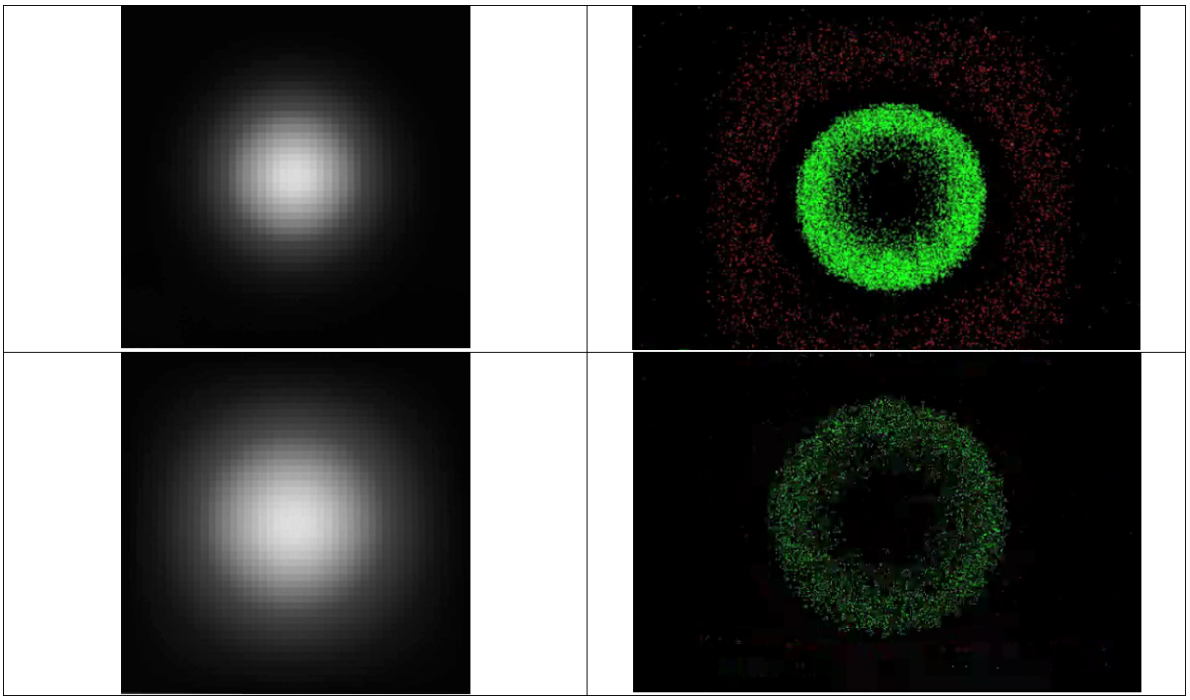

Fig. 14 The monitor-displayed image (photographed on left) is displayed next to examples of the DVXplorer silicon retina imager events, which produces the events shown on the right. Note that the images on the left are not strictly synchronized with the event data on the right.

Conclusion

This work demonstrates a proof-of-concept for the use of event-based imagers for enabling two-color pyrometer imagery in circumstances that would involve a high light intensity environment that cannot be directly observed using conventional 8 bit imagers. Such high intensity light environments are commonly encountered for in-process monitoring of welding as well as metal additive manufacturing. A proof-of-concept of neuromorphic two-color pyrometry has been demonstrated both in simulation as well as with an experimental prototype. The experimental implementation of the neuromorphic two-color pyrometer currently consolidates the response across many pixels as opposed to capturing an image. In order to capture an image associated with temperature change it appears it will be necessary to calibrate out variations in the response of individual pixels. However, the simulation of the event-imaging two-color pyrometer does provide evidence the concept for an event-driven neuromorphic imager is feasible. Future work will consider how variations in response across the pixels can be accounted for to get better estimates of temperature change at high spatial resolution across the full field of view. Variants of the proposed neuromorphic two-color pyrometer could also find application in use cases such as dynamic in-process monitoring of flame temperature during biomass combustion for the generation of clean energy [14], [15].

Acknowledgments Funds for this work were provided by the Los Alamos National Laboratory Technology Evaluation & Demonstration program. Los Alamos National Laboratory is operated by Triad National Security, LLC, for the National Nuclear Security Administration of US Department of Energy (Contract No. 89233218CNA000001). The DVS/DAVIS technology was developed by the Sensors group of the Institute of Neuroinformatics (University of Zurich and ETH Zurich), which was funded by the EU FP7 SeeBetter project (grant 270324).

References

1. A. S. Morris and R. Langari, "Two-color pyrometer (ratio pyrometer)," in Measurement and Instrumentation: Theory and Application, Elsevier Inc., 2012, pp. 347–396.W409W10080
2. J. Dixon, "Industrial radiation thermometry," Journal of Measurement and Control, vol. 20, no. 6, pp. 11–16, 1987. W409W10080
3. S. A. Reggeti, A. K. Agrawal and J. A. Bittle, "Two-color pyrometry system to eliminate optical errors for spatially resolved measurements in flames," Applied Optics, vol. 58, no. 32, pp. 8905–8913, 2019. W409W10080

4. H. Hottel and F. P. Broughton, "Total Radiation from Luminous Gas Flames," Industrial & Engineering Chemistry Analytical Edition, vol. 4, no. 2, pp. 166–175, 1932. W409W10080
5. A. J. Myers, G. Quirarte, F. Ogoke, B. M. Lane, S. Z. Uddin, A. B. Farimani, J. L. Beuth and J. A. Malen, "High-resolution melt pool thermal imaging for metals additive manufacturing using the two-color method with a color camera," Additive Manufacturing, vol. 73, no. 103663, 2023. W409W10080
6. P. Lichtsteiner, P. C. and D. T., "A 128 x 128 120 dB 15 μs Latency Asynchronous Temporal Contrast Vision Sensor," IEEE J. Solid-State Circuits, vol. 43, no. doi:10.1109/JSSC.2007.914337, pp. 566–576, 2008. W409W10080
7. Inivation, "Specifications - Current Models," 2022. [Online]. Available: https://inivation.com/wp-content/uploads/2023/02/2022-09-iniVation-devices-Specifications.pdf. [Accessed 12 May 2023].W409W10080
8. A. Gothard, D. Jones, A. Green, M. Torrez, A. Cattaneo and D. Mascareñas, "Digital coded exposure formation of frames from event-based imagery," Neuromorphic Computing and Engineering, vol. 2, no. 014005, 2022. W409W10080
9. Xiris, "Solutions for Weld Inspection and Monitoring," [Online]. Available: https://www.xiris.com/. [Accessed 20 September 2023].W409W10080
10. C. Schelle, Artist, Event-Based Image of Office Scene. [Art]. Los Alamos National Laboratory, 2018. W409W10080
11. D. Joubert, A. Marcireau, N. Ralph, A. Jolley, A. v. Schaik and G. Cohen, "Event Camera Simulator Improvements via Characterized Parameters," Front Neurosci., vol. 15, no. 702765, 2021. W409W10080
12. H. Rebecq, D. Gehrig and D. Scaramuzza, "ESIM: an Open Event Camera Simulator," in Conf. on Robotics Learning (CoRL), 2018. W409W10080
13. Y. Hu, S.-C. Liu and T. Delbruck, "v2e: From Video Frames to Realistic DVS Events," in IEEE/CVF Conference on Computer Vision and Pattern Recognition Workshops (CVPRW), 2021. W409W10080
14. W. Yan, K. Li, X. Huang, L. Yu, C. Lou and Y. Chen, "Online Measurement of the Flame Temperature and Emissivity during Biomass Volatile Combustion Using Spectral Thermometry and Image Thermometry," Energy and Fuels, vol. 34, no. 1, pp. 907–919, 2020. W409W10080
15. J. P. Silva, S. Teixeira, É. Grilo, B. Peters and J. C. Teixeira, "Analysis and monitoring of the combustion performance in a biomass power plant," Cleaner Engineering and Technology, vol. 5, no. 100334, 2021. W409W10080